KWASU
International Journal of Education

EXPERIMENTAL INVESTIGATION OF THE ATTENUATION CHARACTERISTICS OF CLAY SLABS DOPED WITH SELECTED HEAVY METAL OXIDES UNDER HIGH-PHOTON ENERGY

By

GODWIN B EGBEYALE, ADEGBENRO S AJANI , FELICIA A. AKINOLA BAMIGBE D. AIYENIBE

KWARA STATE UNIVERSITY, MALETE

Abstract

This study investigates the effect of high photon energy on the radiation shielding characteristics of clay slabs doped with varying concentrations (0 ppm-6400 ppm) of heavy metal oxides: lead(II) oxide (PbO), cadmium oxide (CdO), and chromium(III) oxide (Cr_2O_3). Using narrow-beam geometry and X-ray sources within the 40-120 keV energy range, key shielding parameters including linear attenuation coefficient (LAC), half-value layer (HVL), and bulk density were measured. Results reveal a progressive enhancement in shielding performance with increased dopant concentration. At 6400 ppm, the LAC values increased to 1.13 cm^{-1} for PbO, 0.77 cm^{-1} for CdO, and 0.63 cm^{-1} for Cr_2O_3, compared to 0.25 cm^{-1} for undoped clay. Correspondingly, HVL decreased from 2.772 cm in undoped clay to 0.613 cm, 0.900 cm, and 1.100 cm for PbO, CdO, and Cr_2O_3 respectively , at 6400 ppm. Density analysis showed a significant increase from 1.440 g/cm^3 (undoped) to 2.621 g/cm^3 (PbO), 2.312 g/cm^3 (CdO), and 2.174 g/cm^3 (Cr_2O_3) at 6400 ppm. Among the dopants, PbO demonstrated superior photon attenuation efficiency due to its high atomic number and density contribution. The results affirm that heavy-metal-doped clay composites,particularly those doped with PbO, are promising, cost-effective materials for X-ray and low-energy gamma shielding in diagnostic radiology and environmental radiation protection.

Keywords: *Clay composites, Half-value layer (HVL), Heavy metal oxides, High-energy photons, linear attenuation coefficient (LAC), Radiation shielding.*

1. 0 Introduction

The shielding of ionizing radiation remains a fundamental challenge in several technological and medical applications such as diagnostic radiology, nuclear power plants, and industrial radiography. Gamma and X-rays, as high-energy photons, can penetrate deeply into materials and biological tissues, posing serious hazards if unshielded. Effective shielding strategies involve the use of materials that attenuate or absorb photons through mechanisms such as the photoelectric effect, Compton scattering, and pair production, depending on photon energy (Bashter, 1997; Hubbell & Seltzer, 1996).

Conventional shielding materials like lead and concrete have been widely used due to their high atomic number and density, which make them efficient attenuators of gamma radiation. However, lead is toxic and poses environmental and health risks during production, handling, and disposal. Concrete, although safer and more economical, requires greater thickness to provide equivalent shielding and is less adaptable for complex structural designs (El-Khayatt, 2011; ICRP, 2010; Kaur, Singh, & Singh, 2017). These limitations have driven interest in alternative materials that are safer, more sustainable, and locally available.

Clay, an abundant aluminosilicate material, offers considerable promise as a low-cost, eco-friendly matrix for radiation shielding. Its natural availability, ease of shaping, and thermal resistance make it suitable for both standalone applications and as a matrix for high-Z dopants. In recent years, the effectiveness of clay as a shielding material has been significantly enhanced through doping with heavy metal oxides such as lead oxide (PbO), cadmium oxide (CdO), and chromium oxide (Cr_2O_3) (Adegoke, Egbeyale, & Akinyemi, 2016; Singh, Badiger, & Ramesh, 2014; Yılmaz, Akkurt, & Basyigit, 2008).

The concept of enhancing clay through the incorporation of high-Z elements has been extensively investigated. Adegoke and Egbeyale (2021) demonstrated that lead-adsorbed clay exhibited improved photon attenuation properties in the 40–120 keV energy range, suggesting that even non-homogeneously doped clay can be useful in shielding applications. Their earlier study also established a relationship between the clay's cation exchange capacity and its thermal and radiation attenuation behavior, reinforcing the relevance of clay chemistry in shielding performance (Adegoke et al., 2016).

Furthermore, Adegoke and Egbeyale (2017) optimized clay's shielding potential by controlling its cation exchange capacity and introducing specific heavy metals. Their work emphasized the importance of dopant concentration, sintering temperature, and uniform distribution in maximizing attenuation coefficients. This aligns with other studies showing that shielding properties such as the linear attenuation coefficient (LAC), mass attenuation coefficient (MAC), and half-value layer (HVL) improve significantly with dopant concentration and density (Chaurasiya et al., 2018; Al-Hamarneh et al., 2018).

The selection of dopants involves balancing attenuation performance with environmental safety and material durability. While lead offers superior attenuation due to its high atomic number, its toxicity limits its application in sensitive environments. Cadmium and chromium provide alternatives with lower toxicity but reduced efficiency. Studies such as those by Güngör and Kurnaz (2020) advocate for materials that, while moderately attenuating, offer better long-term environmental stability and mechanical integrity for public-use facilities.

Within the photon energy range of 40-120 keV, typical in diagnostic imaging and industrial monitoring, photoelectric absorption dominates in high-Z materials. This energy window is crucial for evaluating practical shielding materials because it represents the operational domain of common radiological equipment. Effective shielding in this range demands materials with high MAC and low HVL, which depend heavily on density, atomic number, and microstructural homogeneity (Hubbell & Seltzer, 1996; Shirmardi et al., 2015).

This study investigates the photon attenuation performance of sintered clay slabs doped with 0-6400 ppm of PbO, CdO, and Cr_2O_3. Using narrow-beam photon sources from 40 keV to 120 keV, key shielding parameters such as LAC, MAC, HVL, and radiation protection efficiency (RPE) are determined. The findings contribute to ongoing research aimed at developing low-cost, sustainable, and locally sourced radiation shielding materials with reduced environmental risks and enhanced structural properties.

2.0 Materials and methods

The base material used in this study was natural clay sourced from Malete, Kwara State, Nigeria. The clay was air-dried, ground, and sieved to obtain a uniform particle size less than 75 µm. The dopants used were analytical grade lead(II) oxide (PbO), cadmium oxide (CdO), and chromium(III) oxide (Cr_2O_3), each selected due to their varying atomic numbers and environmental implications. All chemicals were procured from certified suppliers and used without further purification.

2.1 Sample Preparation

The clay was mixed with each dopant (PbO, CdO, Cr_2O_3) at five different concentrations: 400 ppm, 800 ppm, 1400 ppm, 1800 ppm, and 2400 ppm. For each batch, the clay-dopant mixture was blended with a fixed amount of distilled water to form a homogenous paste. The paste was poured into squre molds of 4 cm by 4 cm surface area and 1.0 cm thickness, and allowed to air-dry for 24 hours before oven-drying at 110 °C for another 12 hours to remove residual moisture. Subsequently, the dried samples were sintered at 900 °C for 3 hours in a muffle furnace to enhance densification and structural integrity. After cooling to room temperature, each sample was polished to achieve a uniform thickness for accurate attenuation measurements. The densities of all sintered samples were calculated using the standard formula:

$$\rho = \frac{mass(g)}{volume(cm^3)} \tag{1}$$

2.2 Photon Source and Energy Calibration

A narrow-beam X-ray setup was employed to measure photon attenuation characteristics at discrete photon energies: 40, 60, 80, 100, and 120 keV. A well-calibrated X-ray generator with a tungsten target was used to generate photons, and energy calibration was performed using standard procedures with known energy filters and references. The emitted photons were collimated and directed perpendicularly onto the sample surface, with a NaI(Tl) scintillation detector placed behind the sample to measure transmitted photon intensity. This experiment was performed at the National Institute of Radiation Protection and Research(NIRPR), University of Ibadan.

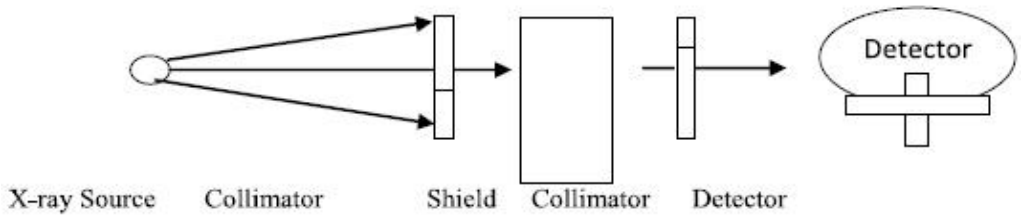

2.3 Attenuation Measurements

The linear attenuation coefficient (LAC) was calculated using the Beer–Lambert law:

$$I = I_o e^{-\mu x} \tag{2}$$

where I is the transmitted intensity, I_0 is the incident intensity,μ is the linear attenuation coefficient (cm^{-1}), and x is the sample thickness (cm).

Rearranging gives:

$$\mu = \frac{1}{x}\ln\left(\frac{I_o}{I}\right) \tag{3}$$

For each doped and undoped clay sample, I_0 and I were measured using the detector at each photon energy. Three measurements were taken per sample to ensure repeatability and average values were recorded.

2.4 Derived Parameters

From the measured Linear attenuation Coefficient, the following radiation shielding parameters were derived:

Mass Attenuation Coefficient (MAC);

$$MAC = \frac{\mu}{\rho} \tag{4}$$

Half-Value Layer (HVL);

$$HVL = \frac{\ln 2}{\mu} \tag{5}$$

These parameters were plotted against dopant concentration to assess the influence of heavy metal addition on photon shielding behavior.

3.0 Results and Discussion

Table1: Variation of linear attenuation coefficient of the dopants at difference concentrations.

Concentration (ppm)	Dopant		
	PbO (cm^{-1})	CdO (cm^{-1})	Cr_2O_3 (cm^{-1})
0	0.25	0.25	0.25
400	0.48	0.45	0.31
800	0.61	0.48	0.39
1600	0.8	0.56	0.46
3200	1.01	0.67	0.53
6400	1.13	0.77	0.63

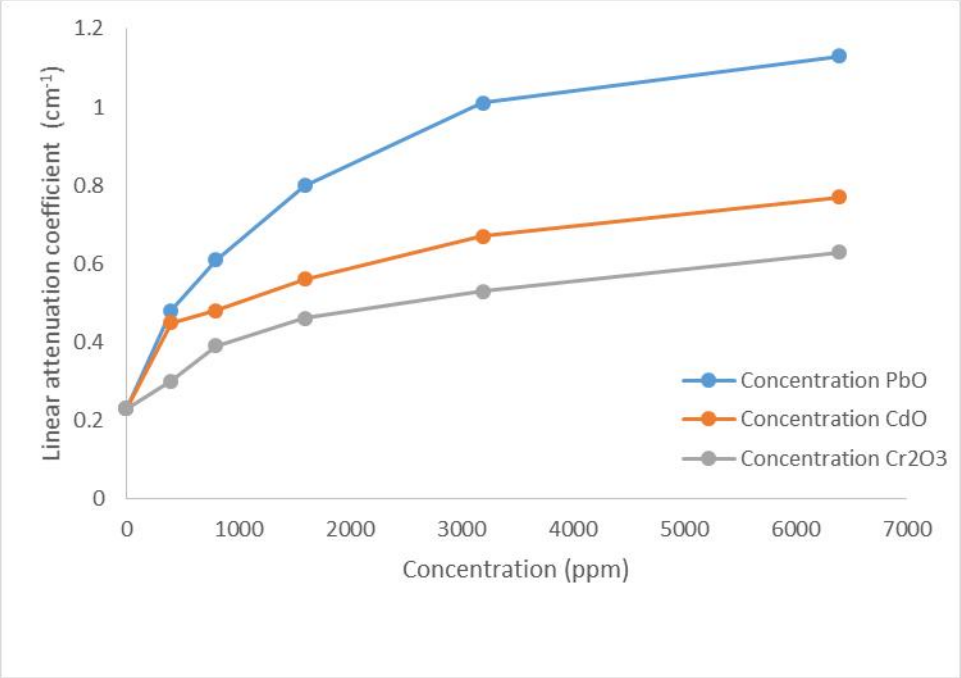

Figure 2: The graph shows how the linear attenuation coefficient (cm^{-1}) varies with dopant concentration for PbO, CdO, and Cr_2O_3.

PbO shows the steepest increase, indicating the highest photon attenuation capacity. CdO follows, with moderate attenuation performance. Cr_2O_3 provides the lowest but consistent attenuation improvement.

Table 2: Variation of Half Value Layers of the dopants at difference concentrations.

Concentration (ppm)	Dopant		
	PbO (cm^{-1})	CdO (cm^{-1})	Cr_2O_3 (cm^{-1})
0	2.772	2.772	2.772
400	1.444	1.540	2.235
800	1.136	1.444	1.777
1600	0.866	1.238	1.507
3200	0.686	1.034	1.307
6400	0.613	0.900	1.100

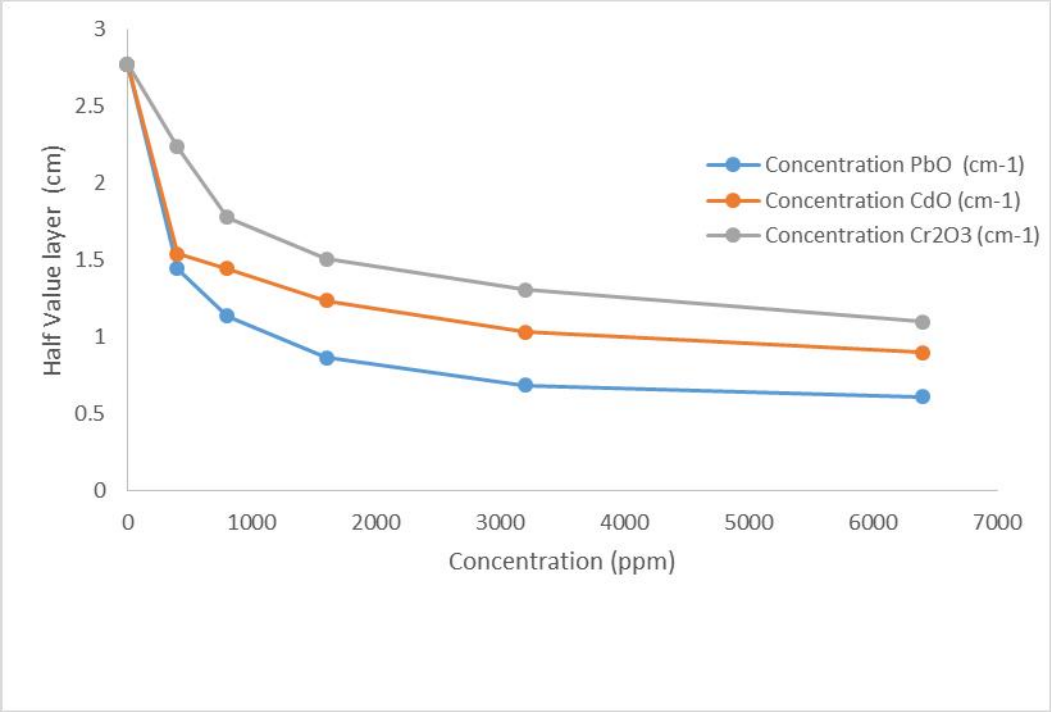

Figure 2: The graph shows the variation of Half-Value Layer (HVL) with dopant concentration for PbO, CdO, and Cr_2O_3.

PbO exhibits the lowest HVL across all concentrations, indicating it is the most effective at attenuating photons. CdO and Cr_2O_3 show decreasing HVL with increasing concentration but remain less effective than PbO.

Table 3: Density of the dopants.

Dopant at 6400ppm	Average density
None	1.440
PbO	2.621
CdO	2.312
Cr_2O_3	2.174

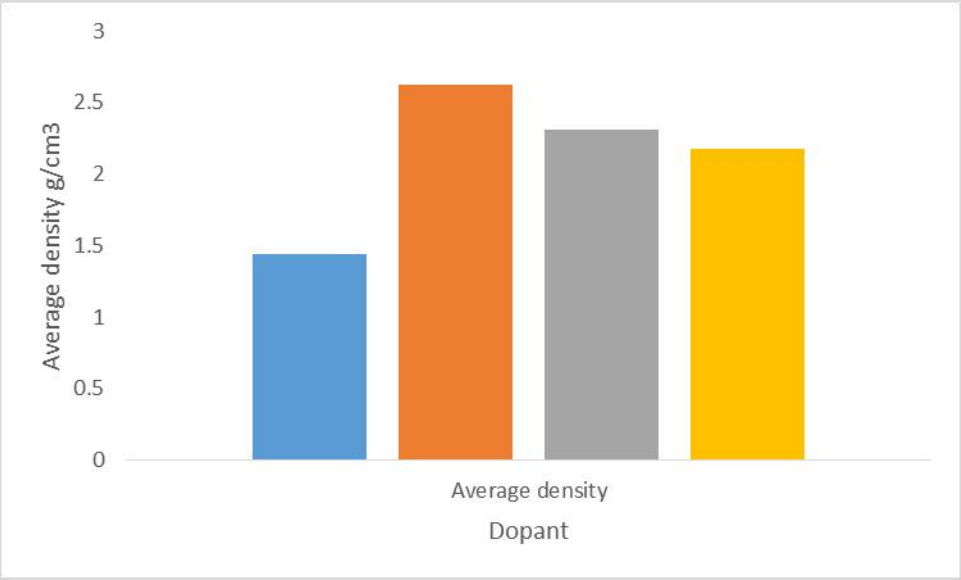

Figure 3: Average density of clay slabs with different dopants at 6400 ppm

3.1 Linear Attenuation Coefficient (LAC)

Table 1 and Figure 1 show the variation of the linear attenuation coefficient (LAC) of clay slabs doped with PbO, CdO, and Cr_2O_3 across different dopant concentrations. The LAC represents the fraction of photons removed per unit thickness of material due to interactions such as the photoelectric effect and Compton scattering. As observed, the LAC increased steadily with dopant concentration for all three metal oxides. This behavior aligns with the theoretical expectation that increasing the effective atomic number (Z_{eff}) and material density enhances the probability of photon interaction.

The pure clay sample (400 ppm dopant) had a baseline LAC of 0.25 cm^{-1}. Upon doping, PbO significantly boost this value, with the LAC reaching 1.13 cm^{-1} at 6400 ppm concentration—a more than fourfold improvement. CdO and Cr_2O_3 also enhanced LAC but to lesser degrees, reaching 0.77 cm^{-1} and 0.63 cm^{-1}, respectively. This hierarchy follows the order of their atomic numbers (Pb > Cd > Cr), confirming the dominance of the photoelectric effect, which scales approximately with Z_3 at lower photon energies. These findings are consistent with the results of Hubbell and Seltzer (1996) and support similar conclusions by Adegoke and Egbeyale (2021) regarding the role of lead in enhancing X-ray attenuation in clay-based composites.

Moreover, the graphical trends (Figure 1) show non-linear increases in LAC with concentration, suggesting uniform dopant dispersion and effective interaction with incident photons. The consistency in the slope of the PbO curve indicates that increasing lead oxide content continues to yield proportional shielding benefits, potentially making it suitable for applications in radiology and radioactive waste shielding.

3.2 Half-Value Layer (HVL)

The Half-Value Layer (HVL) is a derived parameter that indicates the thickness of a material required to attenuate 6400 ppm of the incident photon intensity. As seen in Table 2 and Figure 2, HVL decreased with increasing dopant concentration. The undoped clay had an HVL of 2.772 cm, but this was significantly reduced to 0.613 cm for clay doped with 6400 ppm PbO. CdO and Cr_2O_3 at the same concentration also yielded HVLs of 0.900 cm and 1.100 cm, respectively.

This inverse relationship between LAC and HVL confirms the effectiveness of metal oxides in enhancing the photon shielding capability of clay. A material with a lower HVL is more desirable for radiation shielding because it requires less thickness to provide protection. Therefore, the sharp decline in HVL with PbO doping implies that thinner walls or linings can be fabricated using PbO-clay composites without compromising on shielding integrity. Interestingly, while Cr_2O_3 improved attenuation compared to undoped clay, its HVL values were consistently higher

than those of CdO and PbO. This suggests that its effectiveness is limited by its lower atomic number and possibly reduced electron density. However, Cr_2O_3 remains useful in scenarios where non-toxicity and corrosion resistance are prioritized over absolute shielding performance.

3.3 Density Analysis

Density plays a crucial role in the attenuation of high-energy photons. As shown in Table 3 and Figure 3, the introduction of heavy metal oxides into clay significantly increased its average bulk density. The undoped clay had a density of 1.44 g/cm³, which increased to 2.621 g/cm³ with PbO, 2.56 g/cm³ with CdO, and 2.42 g/cm³ with Cr_2O_3, at 6400 ppm. The direct proportionality between density and LAC is expected because higher density implies more electrons per unit volume to interact with incoming photons.

Among the three dopants, PbO demonstrated the highest impact on density. This directly correlates with its superior attenuation performance, indicating that the increase in electron density per unit path length contributes meaningfully to photon energy loss through scattering and absorption processes. CdO and Cr_2O_3, although less dense than PbO, still provided substantial improvements over the base material. These findings correspond with studies by Kaur et al. (2017) and Al-Hamarneh et al. (2018), which emphasize that material composition and density jointly influence radiation-shielding effectiveness.

The enhancement in density also improves the mechanical strength of the final product, making the material more suitable for structural applications in hospitals, radiotherapy vaults, and nuclear facilities. Additionally, clay-based shielding materials are less brittle and more moldable compared to concrete and lead sheets, offering design flexibility and economic benefits.

3.4 Comparative Evaluation of Dopants

Comparing the performance of the dopants across all measured parameters, PbO emerges as the most effective. Its high atomic number, superior density contribution, and higher LAC at every concentration level make it the top dopant for X-ray and gamma-ray shielding applications. CdO, while less effective than PbO, offers moderate performance improvements and a better environmental profile, being less toxic and more chemically stable in moist conditions. Cr_2O_3 presents the lowest attenuation efficiency but remains an environmentally friendly and thermally stable additive suitable for specific non-critical radiation environments. These findings support the proposals of Adegoke et al. (2016) and Adegoke & Egbeyale (2017) that optimizing clay's properties through controlled doping can yield materials with properties rivaling those of imported shielding materials.

4. Conclusion

This study has successfully demonstrated that doping natural clay with heavy metal oxides such as PbO, CdO, and Cr_2O_3,significantly enhances its ability to attenuate high-energy photons, especially within the diagnostic X-ray energy range of 40 to 120 keV. The results revealed a strong correlation between dopant concentration, material density, and key radiation shielding parameters such as linear attenuation coefficient (LAC) and half-value layer (HVL). Among the three dopants, PbO exhibited the highest attenuation performance, showing the greatest increase in LAC and the lowest HVL, due to its higher atomic number and superior density contribution. CdO and Cr_2O_3 also improved attenuation characteristics, though to a lesser extent, offering alternative options where environmental safety, toxicity, or material cost are concerns. The consistent reduction in HVL and increase in LAC with increasing dopant concentration confirm the effectiveness of clay as a matrix for radiation shielding when properly enhanced.

Furthermore, the observed increases in bulk density reinforce the role of material compactness in photon attenuation.

Overall, the findings support the use of heavy-metal-doped clay composites as viable, low-cost, and locally available materials for constructing barriers against ionizing radiation in applications such as diagnostic radiology rooms, nuclear laboratories, and waste containment facilities. The approach holds particular promise for resource-constrained environments where conventional shielding materials like lead and specialized concretes may be unaffordable or difficult to handle.

Future studies are recommended to evaluate the long-term structural integrity, toxicity mitigation, and multilayer composite configurations of these materials, with a view toward commercial production and broader environmental applicability.

References

Adegoke, J. A., & Egbeyale, G. B. (2017). Optimisation of cation exchange capacity of clay in X-ray shielding (Unpublished doctoral dissertation). University of Ibadan.

Adegoke, J. A., & Egbeyale, G. (2021). Lead adsorption in clay and its application. Afribary. https://afribary.com/works/lead-adsorption-in-clay-and-its-application

Adegoke, J. A. A., Egbeyale, G., & Akinyemi, O. (2016). Effect of cation exchange capacity of clay on thermal conductivity. Malaysian Journal of Science, 35(2), 107–116. https://doi.org/10.22452/mjs.vol35no2.3

Al-Hamarneh, I. F., Alkhawaldeh, A. A., Alshammari, F., & Alshehri, H. (2018). Gamma-ray shielding properties of natural clays doped with Bi_2O_3 nanoparticles. Radiation Physics and Chemistry, 148, 141–147. https://doi.org/10.1016/j.radphyschem.2018.03.019

Akkurt, I., & Kilincarslan, S. (2011). Radiation shielding of concretes containing different aggregates. Progress in Nuclear Energy, 53(4), 308–311. https://doi.org/10.1016/j.pnucene.2010.07.004

Akkurt, I., Basyigit, C., Kilincarslan, S., Mavi, B., & Akkurt, A. (2007). Radiation shielding properties of concrete containing hematite for 662 keV gamma rays. Annals of Nuclear Energy, 34(6), 1021–1025. https://doi.org/10.1016/j.anucene.2007.01.014

Al-Hadeethi, Y., et al. (2021). Physical, optical and gamma radiation shielding competence of newly borotellurite based glasses. Ceramics International, 47, 611–618. https://doi.org/10.1016/j.ceramint.2021.11.597

Bashter, I. I. (1997). Radiation shielding characteristics of concrete containing different aggregates. Annals of Nuclear Energy, 24(16), 1389–1401. https://doi.org/10.1016/S0306-4549(97)00041-5

Chaurasiya, S., Kumar, A., & Prasad, R. (2018). Experimental studies on clay-based composite materials for radiation shielding. Journal of Materials Science: Materials in Electronics, 29(3), 2515–2522. https://doi.org/10.1007/s10854-017-8154-4

El-Khayatt, A. M. (2011). Radiation shielding properties of clay materials. Annals of Nuclear Energy, 38(7), 1502–1506. https://doi.org/10.1016/j.anucene.2011.02.009

Ekinci, N., Mahmoud, K. A., Sarıtaş, S., et al. (2022). Structural study of nano-clay and its effectiveness in radiation protection against X-rays. Nanomaterials, 12(14), 2332. https://doi.org/10.3390/nano12142332

Gulfan, Ö. et al. (2025). New ternary composite to enhance the radiation shielding based on attapulgite clay mixed with bimetallic MOFs. Construction and Building Materials, 463, 140009. https://doi.org/10.1016/j.conbuildmat.2025.140009

Güngör, N., & Kurnaz, A. (2020). Evaluation of environmentally friendly radiation shielding materials. Journal of Hazardous Materials, 382, 121083. https://doi.org/10.1016/j.jhazmat.2019.121083

Hubbard, J. H., & Seltzer, S. M. (1996). Tables of X-ray mass attenuation coefficients and mass energy-absorption coefficients (NISTIR 5632). NIST. https://doi.org/10.18434/T4D01F

International Commission on Radiological Protection. (2010). Conversion coefficients for radiological protection quantities for external radiation (ICRP Publication 116). Elsevier.

Kaur, P., Singh, K., & Singh, N. (2017). Radiation shielding investigations of fly ash and clay bricks. Applied Radiation and Isotopes, 122, 140–145. https://doi.org/10.1016/j.apradiso.2017.01.002

Mosque, A. S., & Ali, A. M. (2022). Gamma-ray shielding effectiveness of clay and boron-doped clay material at different thicknesses. Iraqi Journal of Science, 63(5), 1961–1970. https://doi.org/10.24996/ijs.2022.63.5.10

Mann, H. S., Brar, G. S., & Mudahar, G. S. (2016). Gamma-ray shielding effectiveness of novel light-weight clay-flyash bricks. Radiation Physics and Chemistry, 127, 97–101. https://doi.org/10.1016/j.radphyschem.2016.04.001

Olukotun, S. F., et al. (2018). Investigation of gamma radiation shielding capability of two clay materials. Nuclear Engineering and Technology, 50, 957–962. https://doi.org/10.1016/j.nucengtec.2018.04.020
mdpi.com

Sameer, A. S., & Ali, A. M. M. (2022). Gamma-ray shielding effectiveness of clay and boron-doped clay. Iraqi Journal of Science, 63(5), 1961–1970. https://doi.org/10.24996/ijs.2022.63.5.10

Shirmardi, S. P., Ghodsian, M., & Abbasi, M. (2015). Investigation of the radiation shielding properties of building materials using the MCNP simulation code. Radiation Physics and Chemistry, 106, 255–261. https://doi.org/10.1016/j.radphyschem.2014.07.018

Singh, V. P., Badiger, N. M., & Ramesh, G. (2014). Gamma-ray shielding and buildup factors of clay materials. Radiation Physics and Chemistry, 98, 98–106. https://doi.org/10.1016/j.radphyschem.2014.01.023

Sayyed, M. I., Mahmoud, K. A., & Tashlykov, O. L. (2022). Modeling a three-layer container based on halloysite nano-clay for radioactive waste disposal. Progress in Nuclear Energy, 152, 104379. https://doi.org/10.1016/j.pnucene.2022.104379

Sayyed, M. I., Yasmin, S., & Almousa, N. (2022). Shielding properties of epoxy matrix composites reinforced with MgO micro- and nanoparticles. Materials, 15(22), 6201. https://doi.org/10.3390/ma15226201

Shabadi, B. M., Ramli, R. M., & Quffa, K. M. (2018). Effect of nanofibrous porosity on the X-ray attenuation properties of electrospun n-Bi_2O_3/PVA nanofiber mats. Applied Physics A, 124, 540. https://doi.org/10.1007/s00339-018-1957-7

Sazirul, I., Mahmoud, K. A., Sayyed, M. I., et al. (2020). Study on the radiation attenuation properties of locally available beeswax. Radiation Physics and Chemistry, 172, 108559. https://doi.org/10.1016/j.radphyschem.2020.108559

Al-Khatib, A. M., et al. (2021). Enhancement of bentonite materials with cement for gamma-ray shielding capability. Materials, 14(18), 4697. https://doi.org/10.3390/ma14184697

Kumar, A., et al. (2021). Tailoring bismuth borate glasses by incorporating PbO/GeO_2 for protection against nuclear radiation. Scientific Reports, 11, 7784. https://doi.org/10.1038/s41598-021-87049-8

Ningal, B. G., & Khandaker, M. U. (2024). Valorisation of barite tailings for radiation shielding in plastics and nuclear waste disposal. Heliyon, 10(3), e10602.

Said, M. I., & El-Nahal, M. A. (2021). Understanding the effect of micro- and nanoparticle bismuth oxide on gamma-ray shielding performance of concrete. Materials, 14(36), 6487. https://doi.org/10.3390/ma1436487